Generate vortex point adjustable vortex array based on decentered annular beam pumping

KONGTAO CHEN1, LIXU XU1, AODONG NI1, JIALE TANG1, KAIWEN YI1, FUQIANG JIA1*, DUN QIAO2, KANG LI2, NIGEL COPNER2

[1]*School of Electronic Science and Engineering, Xiamen University, Xiamen, 361005, China*
[2]*Faculty of Computing, Engineering & Science, University of South Wales, Wales, CF37 1DL, UK*
**Corresponding author: jiafq@xmu.edu.cn*

Received XX Month XXXX; revised XX Month, XXXX; accepted XX Month XXXX; posted XX Month XXXX (Doc. ID XXXXX); published XX Month XXXX

An adjustable optical vortex arrays (OVAs) based on decentered annular beam pumping has been demonstrated in an end-pumped Nd:YVO_4 laser. This method allows for not only the transverse mode locking of different modes, but also the ability to adjust the mode weight and phase by manipulating the position of the focusing lens and axicon lens. To explain this phenomenon, we propose a threshold model for each mode. Using this approach, we were able to generate optical vortex arrays with 2-7 phase singularities, achieving a maximum conversion efficiency of 25.8%. Our work represents an innovative advancement in the development of solid-state lasers capable of generating adjustable vortex points.

Vortices have been extensively studied for their special phase singularities, from scalar to vector and from phase singularities to polarisation singularities. Back in 1992, L. Alien et al [1]. discovered that vortices have quantized orbital angular momentum (OAM), and their spiral phase surface is described by $\exp(il\theta)$, where θ is the azimuthal angle, $l\hbar$ is the OAM carried by each photon, l represents the topological charge value, and the positive or negative l determines the spiral direction of the vortex beam wavefront. Due to these properties, vortex beams have attracted increasing attention over the last few decades, and have shown great potential for numerous applications, including high-capacity optical communications [2], rotating object detection [3][4], optical tweezers [5], quantum entanglement [6], and other fields.

However, OVAs with multiple vortices offer more possibilities and flexibility in information encoding and optical manipulation. Compared to pure vortex beams with an annular intensity profile, OVAs have more phase singularities and richer patterns and can increase the information transfer capability in the communication field [7][8]. In addition, OVAs allow for optical manipulation and control of tiny objects, enabling the captured and observation of greater number of particles, which can be applied to biomedical and nanotechnology fields [9]. Various methods have been proposed to generate OVAs, which can be broadly classified as out-of-cavity conversion and direct in-cavity excitation. Out-of-cavity methods involve passing single-mode lasers through holograms generated by spatial light modulators [10], helical phase plates [11], and liquid crystals [12] to generate optical vortices and vortex arrays. These methods provide flexible control of the wavefront of the light, but suffer from reduced efficiency and beam quality. Intracavity methods, on the other hand, typically involve using a circular distribution of pump light to generate OVAs in a solid-state laser. This can be achieved by actively adjusting the pump and gain distribution, such as the pump power, pump distance, and the size of the pump spot on the gain crystal [13][14]. Recently, Dong et al. [15] demonstrated tunable singularity vortex arrays in a microcore laser by manipulating the gain in a Yb:YAG crystal through control of the tilt angle and pump power. They also produced a one-dimensional vortex array with a peak power of 5.56 kW and tunable singularities 1-4 in a microcore laser [16]. Li [17] used a combination of a conical lens and a focusing lens to achieve high-quality of Laguerre-Gaussian (LG) beam with tunable topological charge values up to 18th order, by adjusting the laser power and focusing position. Zhang et al [18] achieved OVAs in Nd:YVO_4 crystals using conical lenses to generate annular pump light, resulting in spontaneous transverse mode locking of LG modes with different frequency simplex families by adjusting the pump power only. They produced vortex arrays of up to four vortices, but their optical conversion efficiency was low, and the vortex arrays were also not sufficiently richly patterned.

In this paper, we generate vortex arrays by exciting them with pump light constructed through a combination of a conical lens and a focusing lens. By adjusting the position of the focusing lens while keeping the power constant, we can change the number of vortex points and their distribution, leading to different vortex array distributions and increasing the output power of the mode.

To obtain these vortex arrays, we solve the paraxial fluctuation equation in a right-angle coordinate system and obtain the standard orthogonal solution, which gives the following expression for LG [18]:

$$LG_{p,l} = \sqrt{\frac{2p!}{\pi(p+|l|)!}}\frac{1}{\omega}\left(\frac{\sqrt{2}r}{\omega}\right)^{|l|} L_p^{|l|}\left(\frac{2r^2}{\omega^2}\right) \times \exp\left(-\frac{r^2}{\omega^2} - ik\frac{r^2}{2R}\right)\exp(-il\ ) \times \exp[-i(2p+|l|+1)\arctan(z/z_R)], \quad (1)$$

Where $L_P^{|1|}(\cdot)$ is the generalized Laguerre polynomial, the radial index p represents the number of radial nodes of the spot, the angular index l is the topological charge of the beam, r, φ and z are the three coordinate variables of the column coordinates, ω is the radius of the spot beam waist, $k = 2\pi/\lambda$ is the wave number correspond to the laser operating wavelength λ, and $z_R = \pi\omega^2/\lambda$ is the Rayleigh length. The mode frequency of LG is determined by the radial and angular indices of its participating modes, i.e. $2p+|l|=1$.

However, the laser output often does not result in a single mode and the combined excitation of these modes leads to the appearance of additional interesting laser modes. In order to simplify the calculations and propose an interpretation of the output of complex modes, the analysis and simulation can be accomplished by using a mode superposition approach [19]:

$$u = \sum_i^n e^{i\theta_i} g_i u_i\ , \quad (2)$$

Where u represents the output light field, and n denotes the number of modes. u_i indicates the ith sub-mode, θ_i and g_i denote the phase and weight. The results of the modes obtained by the superposition are explored below with respect to the phase differences and weights between the superimposed modes.

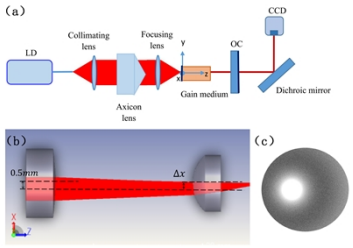

Fig. 1. Experimental device for realizing vortex array with eccentric annular pump light

Figure 1(a) shows our experimental setup. We use an 808 nm fiber-coupled laser diode (LD) with a core diameter of 400 μm, numerical aperture of 0.22, and maximum power of 10 W as the pump source. The pump beam is collimated using a plane convex lens, and then shaped and focused into the gain medium using a conical lens (Thorlabs AX125-B) and a focusing lens with a focal length of 10mm. The resonator has a length of 16 mm. The laser material used in our experiment is a 3 mm × 3 mm × 5 mm a-cut Nd:YVO_4 crystal with 0.5 at. % doping concentration. The crystal is wrapped in indium foil and installed in a copper radiator, with the temperature actively controlled at 12 ℃ using a thermoelectric cooler (TEC) to mitigate thermal effects.

The left side of the laser crystal is coated with a high transmittance coating (HT) at 808 nm and a highly reflective layer (HR) at 1064 nm, which serves as the input mirror to the laser cavity. The right side of the crystal is coated with anti-reflective (AR) coatings at 808 nm and 1064 nm to reduce intracavity losses. The output coupler is a plane-parallel mirror with a reflectivity of 90% at 1064 nm. The output laser is filtered by pump light using a dichroic mirror coated with 808 nm HT and 1064 nm HR films. A CCD camera is used to record the spot size and shape, and a power meter is used to measure the laser energy obtained.

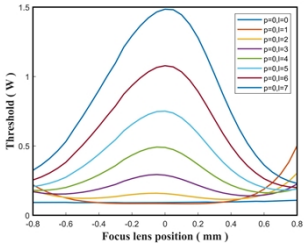

Fig. 2. The change of the threshold of each mode with the position of the focusing lens, l from 0 to 7.

Annular pump light excitation of resonant cavities is a common method of obtaining vortex light to obtain OVAs. The conical lens is a common means of obtaining cyclic pump light due to their unique optical properties and the low loss of pump light shaping in this way. To further alter the symmetry of the pump, the tapered lens is shifted by 0.5 mm relative to the main optical axis of the pump light, as shown in Fig. 1(b), and the focusing lens is shifted by Δx from the main optical axis, with the pump light distributed as shown in the Fig. 1(c). For an end-pumped solid-state laser, the threshold pump power oscillation for a single mode is given as follows [20]:

$$P_{th} = \frac{\gamma I_{sat}}{\eta_p L}\frac{1}{\iiint s(x,y,z)r_p(x,y,z)dv}, \quad (3)$$

Where γ represents the total loss incurred per round trip, is the saturation intensity, and is the length of the gain medium. is the optical transmission efficiency, which is the ratio of the power incident on the gain medium to the power excited by the pump, while is the absorption efficiency, which is the ratio of the power absorbed by the gain medium to the power incident on the gain medium. and represent the laser and pump frequencies, respectively. is the normalized photon density distribution, and is the normalized pump intensity distribution. We have developed a threshold calculation model based on the threshold equation to assess the effect of a change in the focusing mirror on the threshold of each mode. To simplify the model and reduce calculations due to the high absorption of Nd:YVO_4, we simplified the overall pumping region of the crystal to a plane. As shown in Fig. 2, we observed that the threshold value of each mode changes as the focusing mirror is shifted. The threshold of mode is lower when the focus mirror is shifted near 0 mm, while higher-order modes exhibit a trend of lowering and then raising as the focus mirror is shifted to either side. Furthermore, the higher the mode, the farther the lowest point of the threshold is from the 0 mm. The threshold curve is not symmetrical due to the 0.5 mm offset of the conical lens.

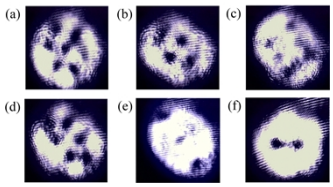

Fig. 3. Modes obtained at different positions of the focusing mirror (a) $\Delta x = 0$ mm, (b) $\Delta x = 0.08$ mm, (c) $\Delta x = 0.25$ mm, (d) $\Delta x = 0.72$ mm, (e) $\Delta x = 0.91$ mm, (f) $\Delta x = 1$ mm.

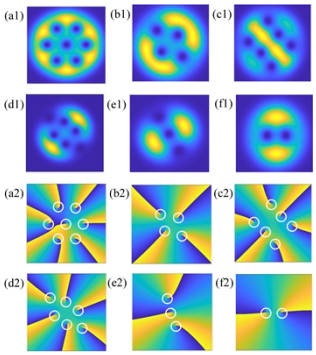

Fig. 4. Simulation of vortex array (a1)$LG_{0,0} + LG_{0,7}$, (b1)$LG_{0,0} + LG_{0,2} + LG_{0,4}$, (c1)$LG_{0,0} + LG_{0,4} + LG_{0,6}$, (d1)$LG_{0,0} + LG_{0,2} + LG_{0,6}$, (e1) $LG_{0,0} + LG_{0,3}$, (f1)$LG_{0,0} + LG_{0,2}$, corresponding phase structures (a2)-(f2).

In our experiments, we kept the pump power constant at 4.2 W and observed different vortex arrays at different positions of the focusing lens. When the focusing lens is not offset ($\Delta x = 0$ mm), the threshold value of the $LG_{0,1}$mode in the threshold graph is lower than the $LG_{0,0}$ mode. The seven-vortex array is observed in the experiment, which is the superposition of $LG_{0,1}$, $LG_{0,7}$. As the focusing lens shifts to the positive direction, the threshold of $LG_{0,2}$, $LG_{0,3}$, $LG_{0,4}$ reaches the minimum value in turn. The output of the four-vortex array is obtained by obtaining the superposition of $LG_{0,0}$, $LG_{0,2}$, $LG_{0,4}$ at 0.08 mm. The superposition of $LG_{0,0}$, $LG_{0,2}$, $LG_{0,6}$ is obtained at 0.25 mm to realize the output of six-vortex array. As the threshold of the $LG_{0,2}$ increases, the threshold of the $LG_{0,4}$ decreases, and the $LG_{0,4}$ starts to dominate. The superposition of $LG_{0,0}$, $LG_{0,4}$, $LG_{0,6}$ is acquired at 0.8 mm to realize the output of the six-vortex array. The threshold of the higher-order mode is further raised, and the lower-order mode begins to take the initiative. The three-vortex array is acquired by the superposition of $LG_{0,1}$, $LG_{0,3}$ at 0.91 mm. The output of the double vortex array is achieved by the superposition of the $LG_{0,0}$, $LG_{0,2}$at Δx =1 mm. The corresponding phase structure is shown in Fig. 4(a2)-4(f2), the individual singularities represented by white circles.

As the focusing lens is moved towards negative values along the x-axis, the number of vortex points decreases. The threshold plots in Fig. 2 show that the threshold of the $LG_{0,1}$ mode increases as the focusing lens is moved towards negative values, and the excitation of the $LG_{0,0}$ mode becomes dominant. When the focusing lens is moved to -0.06 mm, the $LG_{0,0}$, $LG_{0,2}$ and $LG_{0,6}$ modes are observed to be excited, resulting in a six-vortex array. At -0.46 mm, the $LG_{0,1}$ and $LG_{0,3}$ modes become dominant and form a three-vortex array. Further movement of the focusing lens towards negative values, to -0.8 mm, results in the excitation of $LG_{0,0}$ and $LG_{0,2}$ modes, forming the output of a two-vortex array. The corresponding phase structure is shown in Fig. 5(a3)-5(d3).

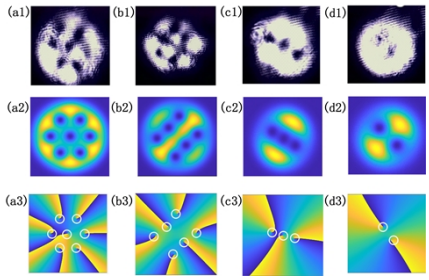

Fig. 5. Modes obtained at different positions of the focusing mirror (a1) $\Delta x = 0$ mm, (b1) $\Delta x = -0.06$ mm, (c1) $\Delta x = -0.46$ mm, (d1) $\Delta x = -0.8$ mm, simulation (a2)$LG_{0,0} + LG_{0,7}$, (b2)$LG_{0,0} + LG_{0,2} + LG_{0,6}$, (c2)$LG_{0,1} + LG_{0,3}$, (d2)$LG_{0,0} + LG_{0,2}$, corresponding phase structures (a3)-(d3).

It can be observed that, although the number of vortices remains the same, the distribution of vortex points differs. This can be attributed to changes in the mode components, as well as variations in the phase and weight of the sub-modes. Specifically, Fig. 4(c1) and (d1) depict the same six-vortex array, but with different arrangements of vortex points. Fig. 4(c1) is composed of $LG_{0,0}$, $LG_{0,2}$ and $LG_{0,6}$, the Fig. 4(d1) is composed of $LG_{0,0}$, $LG_{0,4}$ and $LG_{0,6}$. Besides, the position of vortex points is also can be adjusted. Comparing the two-vortex array in Fig. 4(f1) and Fig. 5(d2), it can be found that the positions of the two-vortex array have changed, and the two-vortex array in Fig. 5(d2) have rotated 45 ° relative to Fig. 4(f1). From the composition of the model, the one in Fig. 4(f1) is $LG_{0,0} + LG_{0,2}$, while the two-vortex array is $LG_{0,0} + \exp(i\pi/2)LG_{0,2}$ in Fig. 5(d2). From Fig. 4(f1) to Fig.5 (d2), the $\theta_{0,2} - \theta_{0,0}$ change from 0 to $\pi/2$. The three-vortex array in Fig. 4(e1) rotates compared with the three-vortex array in Fig. 5(c2), and the spacing between the three-vortex array changes significantly because of the different weights and phase differences of the modes, which can be expressed as $\exp(i\theta_{0,1})g_{0,1}LG_{0,1} + \exp(i\theta_{0,3})g_{0,3}LG_{0,3}$ we calibrate the $\theta_{0,3} - \theta_{0,1} = 3\pi/2$, $g_{0,3}:g_{0,1} = 1:2$ in the Fig. 4(e1), $\theta_{0,3} - \theta_{0,1} = \pi/2$ and, $g_{0,3}:g_{0,1} = 1:1$ in the Fig. 5(c2). In addition to the case of the two-vortex and three-vortex arrays, we also observed this variation in the six-vortex array. Six-vortex arrays with similar vortex point distributions, but at different locations, are found as the focusing lens position is moved from 0.72 mm to 0.8 mm. The six vortex arrays at 0.72 mm and 0.8 mm for the focusing mirror are shown in Fig. 6(a)(d) respectively. For a clearer comparison of the variation in vortex point positions, the distribution of vortex points is shown in Fig. 6(b)(e). The vortex points in six positions are named 1 to 6 respectively. The distance between position 1 and position 6 is set as d_1, and the distance between position 2 and position 5 is set as d_2. After calculation, d_1: $d_2 = 1:0.9$ in Fig. 6(b). $d_1:d_2 = 1:0.9$ in Fig. 6(e). The mode composition of both output modes is $LG_{0,0}$, $LG_{0,4}$ and $LG_{0,6}$. The reason for this position change is that the weight of the $LG_{0,2}$ mode

is reduced. The weights of $LG_{0,0}$, $LG_{0,4}$ and $LG_{0,6}$ are in order $g_{0,0}$, $g_{0,2}$, $g_{0,6}$. The simulation results are shown in Fig. 6(c)(f). The weight distribution of the three modes in Fig. 6(c) is $g_{0,0}$:$g_{0,2}$:$g_{0,6}$ = 1:1:1. The weight distribution of the three modes in Fig. 6 (f) is $g_{0,0}$:$g_{0,2}$:$g_{0,6}$ = 1:0.6:1. The weight of the $LG_{0,2}$ is reduced, which is consistent with the experimental results. The output power changes with the focusing lens as shown in Fig. 7. The maximum output power is 1.084 W when the focusing lens is at 0 mm. The output power decreases as the focusing lens is away from 0 mm. The reason for the power reduction is that the pump light tilts in the gain medium when the focus lens is shifted.

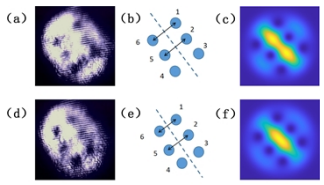

Fig. 6. Six vortex arrays with different mode weight distributions. (a) Experimental results at 0.72mm of the focusing lens, (b) Vortex point distribution (c) Simulation; (d) Experimental results at 0.8 mm of the focusing lens (e) Vortex point distribution (f) Simulation.

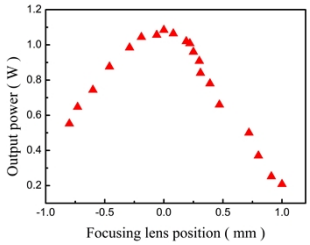

Fig. 7. The output power changes with the position of the focusing lens.

In summary, vortex arrays can be achieved through mode locking, where the number and position of the vortex points are determined by the type of sub-mode they comprise and the weight and phase of the sub-mode. This work uses a combination of a conical lens and a focusing mirror to greatly reduce the energy loss in forming a toroidal pump beam and to expand the number of vortex points in the obtained vortex array. By adjusting the focusing lens, the experiments enable the vortex points to be varied from 2-7, and with some tuning of the vortex point positions, a maximum output power of 1.084 W is achieved, with a maximum conversion efficiency of 25.8%. Our analysis supports the experimental acquisition of vortex arrays. This work represents an innovation in the acquisition of multiple vortex arrays through annular light and provides new ideas for the realization of high-power vortex arrays for lasers. Increasing the pump power is expected to yield more vortex arrays. It has tremendous potential in areas such as particle manipulation and optical communication.

Disclosures. The authors declare no conflicts of interest.

Data Availability. Data underlying the results presented in this paper are not publicly available at this time but may be obtained from the authors upon reasonable request.

Reference

1. L. Allen, M.W. Beijersbergen, R.J.C. Spreeuw, and J.P. Woerdman, "Orbital angular momentum of light and the transformation of Laguerre-Gaussian laser modes." Phys Rev. A **45**, 8185 (1992).
2. D.W. Mackowski, L. Kolokolova, "Application of the multiple sphere superposition solution to large–scale systems of spheres via an accelerated algorithm." J. Quant. Spectrosc. R. A. **287**, 108221 (2022).
3. Y. Ren, S. Qiu, T. Liu, Z. L. Liu, "Compound motion detection based on OAM interferometry." Nanophotonics-Berlin **11**, 1127 (2022).
4. A. Belmonte, C. Rosales-Guzmán, J.P. Torres, "Measurement of flow vorticity with helical beams of light." Optica **2**, 1002 (2015).
5. H.P. Wang, L.Q. Tang, J.N. Ma, H.W. Hao, X.Y. Zheng, D.H. Song, Y. Hu, Y.G. Li, Z.G. Chen, "Optical clearing and shielding with fan-shaped vortex beams." APL Photonics **5**, 016102 (2020).
6. Y.J. Shen, X.J. Wang, Z.W. Xie, C.J. Min, X.Fu, Q. Liu, M.L. Gong, X.C. Yuan, "Optical vortices 30 years on: OAM manipulation from topological charge to multiple singularities." Light-Sci. Appl. **8**, 90 (2019).
7. M. Krenn, R. Fickler, M. Fink, J. Handsteiner, M. Malik, T. Scheidl, R. Ursin, A. Zeilinger, "Communication with spatially modulated Light through turbulent Air across Vienna." New J. Phys. **16** 113028 (2014).
8. S. Franke-Arnold, J. Leach, M. J. Padgett, V. E. Lembessis, D. Ellinas, A. J. Wright, J. M. Girkin, P. Ohberg and A. S. Arnold, "Optical ferris wheel for ultracold atoms." Opt. Express **15** 8619 (2007).
9. L.H. Zhu, M.M. Tang, H.H. Li, Y.P. Tai, X.Z. Li, "Optical vortex lattice: an exploitation of orbital angular momentum." Nanophotonics **10**, 2487 (2021).
10. V.R. Daria, P.J. Rodrigo, J. Gluckstad, "Dynamic array of dark optical traps." Appl. Phys. Lett. **84**, 323 (2004).
11. V.V. Kotlyar, A.A. Almazov, S.N. Khonina, V.A. Soifer, H. Elfstrom, J. Turunen, "Generation of phase singularity through diffracting a plane or Gaussian beam by a spiral phase plate." J. OPT. SOC. AM. A. **22**, 849 (2005).
12. A.Y.G. Fuh, Y.L. Tsai, C.H. Yang, S.T. Wu, "Fabrication of optical vortex lattices based on holographic polymer-dispersed liquid crystal films." Opt. Lett. **43**. 154 (2018).
13. X. Wang, Z.L. Zhang, Y. Gao, S.Y. Zhao, Y.C. Jie, C.M. Zhao, "Investigation on the Formation of Laser Transverse Pattern Possessing Optical Lattices." Front. in Phys-Lausanne **9**, 801196 (2022).
14. W.C. Soares, A.L. Moura, A.A. Canabarro, E. DeLima, J.M. Hickmann, "Singular optical lattice generation using light beams with orbital angular momentum." Opt. Lett. **40**, 5129 (2015).
15. D.M. Chen, Y.J. Miao, H.J. Wang, J. Dong, "Vortex arrays directly generated from an efficient diode-pumped microchip laser." J. Phys-photonics **2**, 035002 (2020).
16. X.C. Wang, S.C. Bai, Y. Pan, B. Lin, J. Dong, "Generation of one-dimensional vortex-arrays with tunable singularity and high peak power in a passively Q-switched microchip laser." Opt. Laser Technol. **143**, 107367 (2021).
17. K. Li, K.F. Tang, D. Lin, J. Wang, B.X. Li, W.B. Liao, Z.L. Lin, G. Zhang, "Direct generation of optical vortex beams with tunable topological charges up to 18th using an axicon." Opt. Laser Technol. **143**, 107339 (2021).
18. S.Q. Zhang, Z.N. Fu, L.Q. Lai, F.Q. Jia, D. Qiao, Y.L. Fan, K. Li, N. Copner, "Transverse mode locking of different frequency-degenerate families based on annular beam pumping." Opt. Lett. **46**, 3195 (2021).
19. Z.L. Zhang, C.M. Zhao, "Spontaneous Phase and Frequency Locking of Transverse Modes in Different Orders." Phys. Rev. Appl. **13**, 024010 (2020).
20. Y.F. Chen, Y.P. Lan, S.C. Wang, "Generation of Laguerre-Gaussian modes in fiber- coupled laser diode end-pumped lasers." Appl. Phys. B **72**, 167 (2001).